Chinese Chemical Letters 37 (2026) 111877

Contents lists available at ScienceDirect

Chinese Chemical Letters

journal homepage: www.elsevier.com/locate/cclet

Bioinspired polyphenols nanoparticles-assembled microneedles integrating antioxidant defense with immune-melanogenic reprogramming for precision vitiligo phototherapy

Wenxiu Hu[a,b,1], Di Liu[a,b,1], Jingxian Gao[a,b], Xinyue Zhang[a,b], Qiqi Zhang[a,b], Lu Han[a,b,*]

[a] Key Laboratory of Marine Drugs, Ministry of Education, Shandong Key Laboratory of Glycoscience and Glycotherapeutic, School of Medicine and Pharmacy, Ocean University of China, Qingdao 266003, China
[b] Laboratory for Marine Drugs and Bioproducts, Qingdao Marine Science and Technology Center, Qingdao 266237, China

ARTICLE INFO

Article history:
Received 5 April 2025
Revised 21 September 2025
Accepted 23 September 2025
Available online 23 September 2025

Keywords:
Microneedles
Polyphenol
Drug delivery
Antioxidative
Immunomodulation

ABSTRACT

Vitiligo is a chronic autoimmune disorder characterized by progressive melanocyte loss. Conventional narrowband ultraviolet B (NB-UVB) phototherapy for vitiligo faces limitations due to reactive oxygen species (ROS)-induced phototoxicity and insufficient melanocyte regeneration in chronic applications. In this study, we propose a differential dual-release bilayer microneedle loaded with two natural plant-derived polyphenols nanoparticles, which integrates rapid antioxidant defense and sustained melanogenic reprogramming for precision vitiligo phototherapy. The upper layer, composed of hyaluronic acid (HA), encapsulates curcumin-fructose self-assembled nanomicelles (CF NMs) for rapid ROS scavenging (68.50% within 15 min), to prevent photodamage and nuclear factor kappa-light-chain-enhancer of activated B cells (NF-κB)-mediated inflammation. The lower gelatin methacryloyl (GelMA) hydrogel layer sustains the release of psoralen-loaded melanin-mimetic mesoporous polydopamine nanoparticles (PMPN), which persistently inhibits the Janus kinase-signal transducer and activator of transcription (JAK-STAT) signaling pathway and reduces autophagy-induced apoptosis, while enhancing tyrosinase activity (0.47-fold increase) to promote melanogenesis. In monobenzone-induced vitiligo mice, the CF/HA-PMPN/GelMA-MNs combined with NB-UVB demonstrated superior outcomes with 80.55% repigmentation at day 14 (*vs.* 25.90% in NB-UVB alone). This "rapid defense-sustained regeneration" paradigm provides a clinically translatable strategy to enhance efficacy and safety in vitiligo phototherapy.

© 2026 Published by Elsevier B.V. on behalf of Chinese Chemical Society and Institute of Materia Medica, Chinese Academy of Medical Sciences.

Vitiligo, an autoimmune disease characterized by depigmentation of the skin and mucous membranes due to the reduction or disappearance of melanocytes, poses a complex pathogenesis [1–3]. Among various contributing factors, the accumulation of oxidative stress plays a crucial role in triggering vitiliginous skin events [4–6], which induces melanocyte dysfunction [3,7] and autophagy [8], consequently leading to the development of hypopigmented or depigmented patches on the skin. Moreover, oxidative stress-induced damage triggers apoptotic bodies in melanocytes [9], and stimulates the release of immune response-related cytokines [4,10], leading to inflammasome and $CD8^+$ T cell overactivation in the skin, culminating in localized melanocyte loss [2,11–13]. While various treatments for vitiligo exist [14], they often lack broad applicability and specificity [15]. For instance, alpha-melanocyte stimulating hormone (α-MSH) may be applied to the vitiliginous skin to promote melanin synthesis [16], or glucocorticoids and calcineurin inhibitors are utilized independently to modulate the immune system [17,18]. However, the absence of consideration for synergistic effects renders these treatments susceptible to relapse and resistant to complete cure.

Besides, restoring melanin deposition in the vitiliginous areas is vital for achieving repigmentation and improving the aesthetic appearance of vitiligo patients. Phototherapy techniques, particularly narrowband ultraviolet B (NB-UVB) phototherapy is generally considered as a first-line treatment to induce repigmentation by stimulating the migration and proliferation of melanocytes and melanocyte precursors [19]. However, frequent NB-UVB phototherapy can generate highly active singlet oxygen or hydroxyl radicals that further damage intracellular lipids, proteins, and nucleic acids, resulting in skin phototoxicity [20,21]. Consequently, combining NB-UVB with adjuvants has been proposed to enhance its efficacy [22].

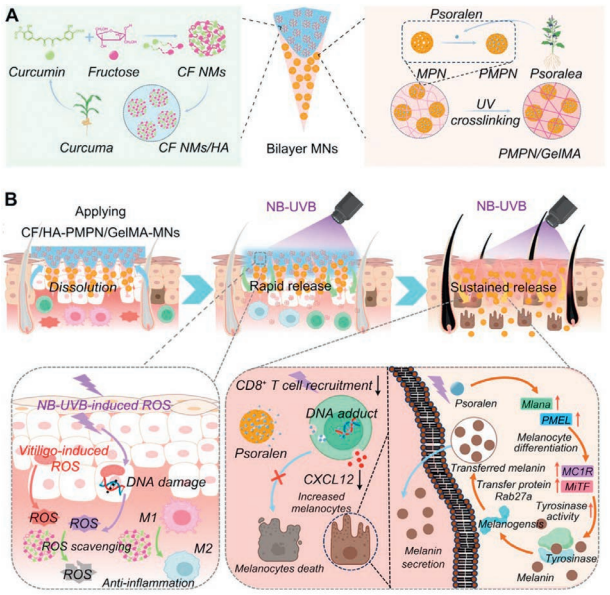
* Corresponding author.
E-mail address: hanlu@ouc.edu.cn (L. Han).
[1] These authors contributed equally to this work.

https://doi.org/10.1016/j.cclet.2025.111877
1001-8417/© 2026 Published by Elsevier B.V. on behalf of Chinese Chemical Society and Institute of Materia Medica, Chinese Academy of Medical Sciences.

Various studies have indicated that bioactive molecules derived from natural compounds possess notable antioxidant and anti-inflammatory properties, offering potential in the treatment of diverse chronic conditions. For example, curcumin (Cur), as a naturally occurring polyphenolic diketone compound with a molecular enol transition, can occur in the α,β-unsaturated β-diketone structure between the two benzene rings, which can scavenge reactive oxygen species (ROS) by electron transfer or hydrogen donation [23,24]. Renowned for its exceptional antioxidant and anti-inflammatory properties [25,26], Cur emerges as a key inducer of the nuclear factor erythroid 2-related factor 2 (Nrf2) antioxidant signaling pathway [27–29], which leads to a substantial reduction in the levels of inflammatory cytokines, such as tumor necrosis factor-alpha (TNF-α), effectively alleviating inflammation symptoms [30,31]. Therefore, Cur can serve as an exceptional antioxidant and anti-inflammatory agent in the fight against NB-UVB-induced inflammation and DNA damage in the skin. Nonetheless, the limited bioavailability and application of Cur stem from its poor hydrophilicity [32]. Another natural derivative, psoralen, belonging to the furanocoumarin group, is a photoactive compound with the ability to regulate the immune-mediated Janus kinase (JAK) signaling pathway associated with inflammatory diseases, thereby preventing the destruction of melanocytes [33]. Psoralen further enhances the phosphorylation of p38 mitogen-activated protein kinase and cyclic adenosine monophosphate, as well as the expression of melanogenic proteins and microphthalmia-associated transcription factor (MiTF) [34,35]. Moreover, psoralen can undergo a photochemical reaction with thymine on epidermal DNA under UVB, forming light adducts that inhibit immune-mediated inflammatory damage to melanocytes, thereby amplifying the pigmentation effect of UVB exposure [36,37]. Despite its therapeutic potential, the poor hydrophilicity and photosensitivity of psoralen also pose challenges to its effective penetration and absorption by the skin.

As a new type of transdermal drug delivery system, microneedles (MNs) can create micron-sized mechanical channels and the loaded drug can achieve deep diffusion in the skin through its dissolution or swelling process [38]. The utilization of MNs enables precise delivery of different drugs to keratinocytes and melanocytes *in situ*, while also modulating various immune processes within the skin and expediting the recovery from autoimmune conditions [39–41]. Among these, bilayer MNs exhibit superior accuracy in drug layer deposition compared to single-layer MNs, presenting novel prospects for personalized and tailored treatment approaches, thus garnering increased interest [42,43]. The distinctive attributes of bilayer MNs can noninvasively deliver different drugs for the management of vitiligo [44].

In this study, we designed a differential dual-release bilayer MN to enhance the effectiveness of NB-UVB phototherapy for vitiligo (Scheme 1). The upper layer of the MN consists of dissolvable hyaluronic acid (HA), facilitating the rapid release of curcumin-fructose self-assembled nanomicelles (CF NMs) that efficiently deplete ROS and inhibit inflammatory responses, which protect against UVB-induced oxidative damage and inflammation in skin, while preserving the therapeutic benefits of NB-UVB treatment. The lower layer of the MN is composed of UV-crosslinked gelatin methacryloyl (GelMA) hydrogel, serving as a long-term depot for the sustained release of psoralen. The melanin-mimicking mesoporous polydopamine nanoparticles (MPN) were used to enhance the stability of psoralen that efficiently targeted the immune-mediated JAK signaling pathway, thereby inhibiting autophagic damage to melanocytes while increasing repigmentation in conjunction with NB-UVB phototherapy. *In vivo* monobenzone-induced vitiligo mouse model demonstrated the synergistic effects of UVB therapy combined with the bilayer MNs, which effectively alleviated oxidative stress, inhibited autophagic damage, and promoted melanin synthesis, without inducing phototoxicity on the skin.



Scheme 1. (A) Schematic diagram of the design of differential dual-release bilayer CF/HA-PMPN/GelMA-MNs and (B) the mechanism of MN-assisted NB-UVB phototherapy in vitiligo treatment.

First, MPN were synthesized by an emulsion-induced interface polymerization method [45–47]. Next, psoralen derived from Psoralea was physically absorbed into the mesopores of MPN to yield psoralen-loaded melanin-mimetic mesoporous polydopamine nanoparticles (PMPN) with a drug encapsulation efficacy of 49.68 % (Fig. 1A). Transmission electron microscopy (TEM) observation further indicated that the synthesized MPN exhibited a spherical and mesoporous structure with a diameter of ~260 nm (Fig. S1 in Supporting information). After psoralen loading, the diameter of PMPN increased to approximately 369 nm (Fig. 1B). The results of dynamic light scattering (DLS) were consistent with TEM measurement. The mesoporous structure of MPN was characterized through nitrogen adsorption/desorption analysis, revealing a specific surface area of 11.49 m^2/g and an average pore volume of 0.048 cm^3/g (Fig. 1C and Fig. S2 in Supporting information). Additionally, Fourier-transform infrared (FTIR) spectroscopy of PMPN revealed an absorption peak corresponding to the C=O stretching vibration of glycosides near 1000 cm^{-1} (Fig. S3 in Supporting information). Furthermore, the cumulative drug release profile of PMPN was investigated in phosphate-buffered saline (PBS, pH 7.4) supplemented with 0.1 % (w/v) Tween-80. As demonstrated in Fig. 1D, the cumulative release of psoralen reached 40.8 % ± 0.4 % after 24 h. Collectively, these findings confirm the successful incorporation of psoralen into the mesopores of MPN, facilitating the effective release of the drug.

Considering the poor water solubility of Cur, the hydrophilic fructose was employed to facilitate co-assembly with Cur (Fig. 1E) [48], resulting in the formation of globular CF NMs with hydrophilic groups on the exterior and hydrophobic groups in the interior in an aqueous medium, exhibiting the Tyndall effect (Fig. S4 in Supporting information). The Cur content in CF NMs was determined to be 37.00 %. TEM analysis revealed that CF NMs exhibited spherical morphology with an average size of approximately 30 nm (Fig. 1F), while DLS measurements indicated a larger hydrodynamic diameter of 234.83 ± 18.17 nm (Fig. S5 in Supporting information). The FTIR spectrum of CF NMs illustrated characteristic peaks of Cur and fructose, including C=C stretching at 1626 cm^{-1}

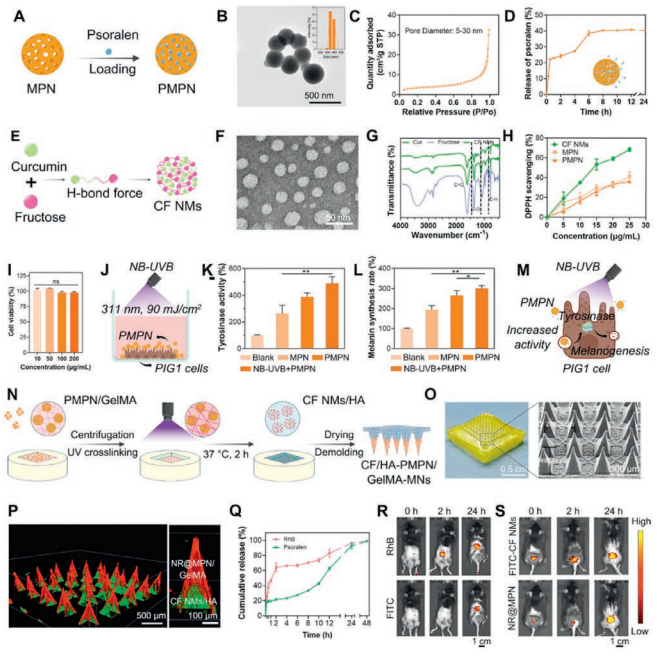


Fig. 1. Characterizations of PMPN, CF NMs and CF/HA-PMPN/GelMA-MNs. (A) Schematic of fabricating PMPN. (B) TEM image of PMPN. (C) The average adsorption rate curve of MPN. (D) *In vitro* release curve of psoralen from PMPN. (E) Schematic of fabricating CF NMs. (F) TEM image of CF NMs. (G) FTIR spectra of fructose, Cur and CF NMs. (H) DPPH scavenging ability of CF NMs, MPN and PMPN. (I) Viability of PIG1 cells after incubation with PMPN at various concentrations for 24 h. (J) Schematic diagram illustrating the experiments to assess the bioactivity of PMPN in promoting tyrosinase activity and melanin synthesis in PIG1 cells under NB-UVB irradiation. (K) Tyrosinase activity and (L) rate of melanin synthesis of PIG1 cells post incubation with MPN, PMPN with or without NB-UVB irradiation (311 nm, 90 mJ/cm^2). (M) Schematic illustration of promoting tyrosinase activity and melanin synthesis in PIG1 cells by PMPN combined with NB-UVB irradiation. (N) Schematics of the fabrication process of CF/HA-PMPN/GelMA-MNs. (O) Appearance and SEM image of CF/HA-PMPN/GelMA-MNs. (P) CLSM images of CF/HA-PMPN/GelMA-MNs and its biolayered structure. (Q) The release curves of RhB (a model drug of Cur) and psoralen from MNs in PBS ($n = 3$). *In vivo* fluorescence images of C57BL/6J mice at 0, 2, and 24 h after insertion of (R) (RhB)/HA-(FITC)/GelMA-MNs (the upper layer of the MNs was loaded with RhB, and the lower layer of the MNs tips was loaded with FITC) or (S) CF(FITC)/HA-MPN(NR)/GelMA-MNs (the upper layer of the MNs was loaded with FITC-labelled-CF NMs, and the lower layer of the MNs was loaded with NR-labelled-MPN). Data are presented as the mean ± SD. ns, no statistical significance. $^*P < 0.05$, $^{**}P < 0.01$.

of Cur, terminal C–H bending at 842 cm^{-1}, C–O stretching near 1100 cm^{-1}, and a broad -OH stretching band at 3000–3600 cm^{-1} of fructose (Fig. 1G). The release kinetics of CF NMs in PBS (pH 7.4) containing 0.1 % (w/v) Tween-80 over a 24-h period showed that approximately 37.11 % ± 0.04 % of Cur was released at 12 h (Fig. S6 in Supporting information). Moreover, both PMPN and CF NMs exhibited DPPH radical scavenging efficiencies of 36.02 % ± 1.44 % and 68.50 % ± 1.93 %, respectively (Fig. 1H), demonstrating their remarkable antioxidative activity.

The primary cells responsible for regulating skin pigmentation are melanocytes, specifically the PIG1 cell line. The cytocompatibility of the CF NMs and PMPN was assessed through cell counting kit-8 (CCK-8) assays on PIG1 cells, showing cell survival rates above 80 % after 24 h of co-incubation (Fig. 1I and Fig. S7 in Supporting information). Confocal laser scanning microscopy (CLSM) further confirmed efficient internalization of both CF NMs and NR@MPN by PIG1 cells (Fig. S8 in Supporting information). Excessive UVB exposure increases intracellular ROS, limiting the efficacy of phototherapy in vitiligo. Employing antioxidants presents a viable strategy to mitigate UV-induced damage [49,50]. Treatment with CF NMs effectively suppressed UVB-induced ROS accumulation in PIG1 cells, demonstrating their cytoprotective antioxidant effect (Fig. S9 in Supporting information).

The PMPN exhibited the pro-melanogenic activity, as evidenced by incubating PIG1 cells with PMPN at a concentration of 100 μg/mL, followed by exposure to NB-UVB light irradiation (311 nm, 90 mJ/cm^2) for 160 s (Fig. 1J). Firstly, the activity of tyrosinase (TYR) was evaluated by using L-Dopa as the substrate. In the presence of TYR, L-Dopa undergoes oxidative conversion to dopachrome [51]. The results revealed that the PMPN combined with NB-UVB irradiation exhibited the highest TYR activity, registering a value that was 1.87 times greater than that observed in the MPN group (Fig. 1K). Subsequently, the effect of the PMPN on melanin pigmentation was investigated by quantifying the melanin content using the sodium hydroxide lytic cell method. The melanin production in the NB-UVB +PMPN group was 1.55 times higher than that in the MPN group (Fig. 1L). Collectively, these findings indicate that the combination of PMPN and NB-UVB irradiation significantly enhances melanin production in PIG1 cells by promoting TYR activity (Fig. 1M).

To achieve smart drug delivery at vitiligo lesion sites, a bilayer MN patch was fabricated for differential drug release through sequential casting (Fig. 1N). The lower layer was made of UV light-cured GelMA hydrogel incorporated with PMPN, and the upper layer was prepared by 10 wt% HA solution mixed with CF NMs. The as-fabricated MNs were denoted as CF/HA-PMPN/GelMA-MNs. The resulting patch (0.0696 cm^2 base area, ~20 mg in weight) contained a 10 × 10 array of needles with each MN precisely delivering 20 μg CF NMs and 0.5 μg PMPN (Fig. 1O). Scanning electron microscopy (SEM) imaging revealed that MNs possessed conical needles of 493.49 μm in height and 208.33 μm in base diameter (Fig. 1O and Fig. S10 in Supporting information). A clear boundary between the HA layer and the GelMA layer was observed in the SEM magnification of the CF/HA-PMPN/GelMA-MNs. To further confirm the bilayer structure of MNs, red Nile Red (NR) was incorporated into MPN to prepare CF/HA-NR@MPN/GelMA-MNs. The CLSM images revealed that the red fluorescence of MPN (NR) was distributed in the lower layer, and the green fluorescence of CF NMs was distributed throughout the upper layer of MN (Fig. 1P), indicating the successful preparation of bilayer MNs. CF/HA-PMPN/GelMA-MNs exhibited sufficient mechanical strength (0.72 N per needle) to penetrate the stratum corneum [42] while maintaining structural integrity *in vivo* (Figs. S11–S13 in Supporting information). CF/HA-PMPN/GelMA-MNs also showed excellent cytocompatibility and long-term skin safety in mice, supporting their suitability for transdermal drug delivery (Figs. S14–S16 in Supporting information).

The sequential drug-release behavior of the biolayer MNs was evaluated both *in vitro* and *in vivo*. *In vitro* release kinetics revealed that 64.24 % ± 5.49 % of Rhodamine B (RhB) in the upper layer of the MNs was released within 2 h, while only 21.72 % ± 1.71 % of psoralen diffused from the lower layer of the MNs (Fig. 1Q), revealing the differential drug release capability of the bilayer MNs. This differential release pattern was further confirmed using an intradermal diffusion model, where the HA layer rapidly dissolved within 5 min to release CF NMs, while the GelMA layer provided sustained NR@MPN release, as evidenced by progressively increasing red fluorescence intensity (Fig. S17 in Supporting information). Moreover, dual-labeled (RhB)/HA-(fluorescein isothiocyanate (FITC))/GelMA-MNs were applied to the skin of a mouse model and observed by IVIS imaging system. As shown in Fig. 1R, RhB from the HA layer was rapidly delivered within 2 h, whereas FITC from the GelMA layer was observed after 24 h. Furthermore, to assess the *in vivo* transdermal delivery of CF NMs and PMPN from MNs, the CF(FITC)/HA-MPN(NR)/GelMA-MNs were applied to the skin of the mouse model and their release profiles were tracked. Animal study was performed with the permission (approval No. OUC-SMP-2023–06–01) of the Laboratory Animal Ethics Committee, College of Medicine, Ocean University of China, in compliance with ex-

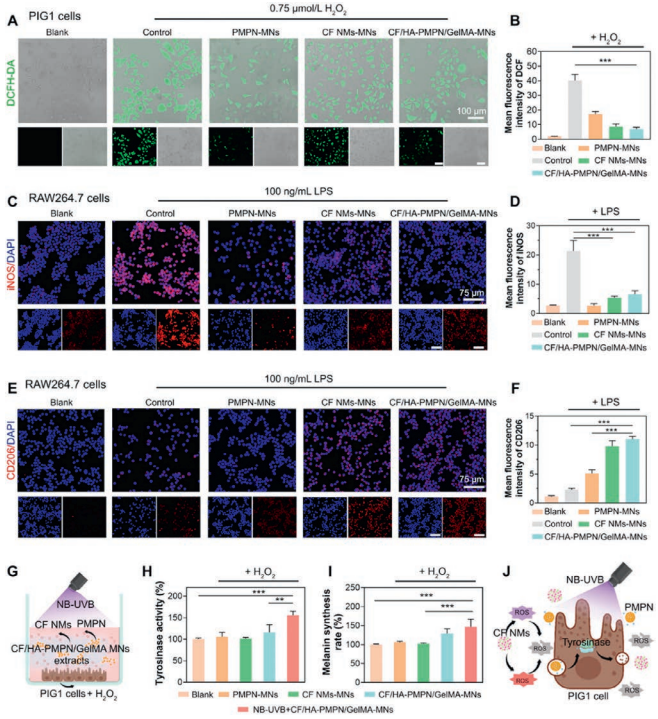


Fig. 2. *In vitro* antioxidant, anti-inflammatory activities, and promoting melanin pigmentation of CF/HA-PMPN/GelMA-MNs under oxidative conditions. (A) Confocal images of H_2O_2-induced PIG1 cells post incubation with different MN extracts, showing the intracellular ROS level with DCFH-DA as the probe. (B) The quantitative analysis of ROS levels in H_2O_2-induced PIG1 cells treated with different MN extracts. (C) Immunofluorescence staining images for iNOS and (D) quantitative analysis of iNOS intensity in RAW264.7 cells treated with different MN extracts. (E) Immunofluorescence staining images for CD206 and (F) quantitative analysis of CD206 intensity in RAW264.7 cells treated with different MN extracts. (G) Scheme of the detection of the TYR activity and melanin synthesis in H_2O_2-induced PIG1 cells co-incubated with different MN extracts under NB-UVB irradiation. (H) TYR activity and (I) rate of melanin synthesis of H_2O_2-induced PIG1 cells post incubation with different MN extracts with or without NB-UVB irradiation (311 nm, 90 mJ/cm^2). (J) Schematic representation of upregulating melanin synthesis in PIG1 cells by CF/HA-PMPN/GelMA-MNs in an oxidative condition. Data are presented as the mean ± SD. $^*P < 0.05$, $^{**}P < 0.01$, $^{***}P < 0.001$.

perimental guidelines of the Laboratory Animal Ethics Committee, College of Medicine, Ocean University of China. Fluorescence imaging revealed distinct temporal release patterns: FITC-labeled CF NMs exhibited rapid release from the HA layer within 2 h (green fluorescence), while NR-labeled MPN initially remained localized (red fluorescence) before gradually dispersing by 24 h (Fig. 1S). This contrasted sharply with control experiments where free FITC-CF NMs and NR@MPN dispersions applied topically were completely cleared from the skin surface within 12 h (Fig. S18 in Supporting information). These findings demonstrate the dual-release mechanism of biolayer MN, where the HA layer enables immediate CF NM delivery and the crosslinked GelMA matrix acts as a sustained-release reservoir for PMPN. This programmed, time-dependent drug release profile underscores the sophistication of this transdermal delivery platform.

Oxidative stress is the initiator of melanocyte degeneration in vitiligo. To analyze the role of CF/HA-PMPN/GelMA-MNs in alleviating oxidative stress, PIG1 cells were incubated with different MN extracts (20 mg/mL) containing 0.75 μmol/L H_2O_2 for 6 h to verify the protective effect of CF NMs in an environment that induces moderate oxidative stress injury in PIG1 cells. As shown in Figs. 2A and B, strong positive staining of intracellular ROS was observed in the H_2O_2-treated control group. Following treatment with extracts of MNs, the cells exhibited decreased intracellular ROS levels, indicating the efficient ROS-scavenging capacity of CF/HA-PMPN/GelMA-MNs, which can protect PIG1 cells from oxidative damage [52–54].

Macrophages represent the paramount cell population within skin tissues, playing an indispensable role in host defense and immunomodulation [55]. The anti-inflammatory properties of CF/HA-PMPN/GelMA-MN extracts were investigated using LPS-stimulated RAW264.7 macrophages. The phenotypic characterization of macrophages across various treatment groups was conducted through immunofluorescence staining for inducible nitric oxide synthase (iNOS, an M1 marker) and cluster of differentiation 206 (CD206, an M2 marker). Following treatment with CF/HA-PMPN/GelMA-MN extracts, a notable reduction in the fluorescence intensity of iNOS was observed (Figs. 2C and D), while the fluorescence associated with CD206 was significantly enhanced (Figs. 2E and F). Quantitative flow cytometry confirmed that CF/HA-PMPN/GelMA-MN extracts significantly downregulated CD86 while upregulating CD206 expression (Figs. S19 and S20 in Supporting information), demonstrating effective immunomodulation through macrophage phenotype switching. Consequently, it can be concluded that CF/HA-PMPN/GelMA-MNs exert a substantial antioxidant and immunomodulatory effect, effectively regulating the homeostasis of the inflammatory microenvironment of vitiligo. A heightened level of oxidative stress has been implicated in eliciting an autoimmune response, ultimately leading to the destruction of melanocytes [56]. To evaluate the efficacy of CF/HA-PMPN/GelMA-MNs in enhancing the pigmenting activity at vitiligo lesion sites when combined with NB-UVB irradiation, PIG1 cells were first incubated with different MN extracts (20 mg/mL) containing 0.75 μmol/L H_2O_2 for 6 h, followed by exposure to NB-UVB light irradiation (311 nm, 90 mJ/cm^2) (Fig. 2G). The pro-TYR activity capacity and pro-melanogenic activity were then measured. The results demonstrated that the CF/HA-PMPN/GelMA-MNs combined with NB-UVB group exhibited a TYR activity escalation, registering at 146.87 % (Fig. 2H), along with a remarkable increase in melanogenesis of 155.78 % (Fig. 2I). Thus, the synergistic application of CF/HA-PMPN/GelMA-MNs and NB-UVB treatment significantly enhanced melanin production in vitiligo microenvironments marked by oxidative stress (Fig. 2J).

The therapeutic efficacy of CF/HA-PMPN/GelMA-MNs was assessed *in vivo* utilizing a monobenzone-induced vitiligo mouse model. In this model, vitiligo lesions manifested on the dorsal surface of C57BL/6J mice after two weeks of treatment with monobenzone dissolved in an ethanol/glycerol mixture (Fig. 3A). The vitiligo-affected mice were randomly divided into five groups ($n = 3$), which included a control group (PBS), a halometasone group (a first-line therapeutic agent for vitiligo), a NB-UVB-irradiated group (UVB), a CF/HA-PMPN/GelMA-MNs group (MN), and a CF/HA-PMPN/GelMA-MNs + NB-UVB irradiated group (MN + UVB). The areas of skin depigmentation in different treatment groups were measured and photographed on days 0, 7, and 14. As shown in Fig. 3B, no significant alteration in the depigmentation area was observed in the control and halometasone groups during 14 days. In contrast, both the UVB group and the MN group demonstrated notable melanin deposition; however, the MN + UVB group exhibited a more accelerated rate of melanin deposition and hair regrowth. Quantitative analysis indicated that the MN + UVB group achieved 80.55 % ± 6.96 % recovery of vitiligo lesions by day 14, which significantly surpassed the recovery rates observed in the UVB group (25.90 % ± 18.03 %) and MN group (34.89 % ± 6.09 %) (Fig. 3C). These results confirmed the synergetic effect of NB-UVB light and CF/HA-PMPN/GelMA-MNs in promoting rapid pigmentation.

The recovery process of vitiligo was further investigated by histological analysis, including Masson Fotana staining and Masson Trichrome staining. The Masson Fontana staining results revealed

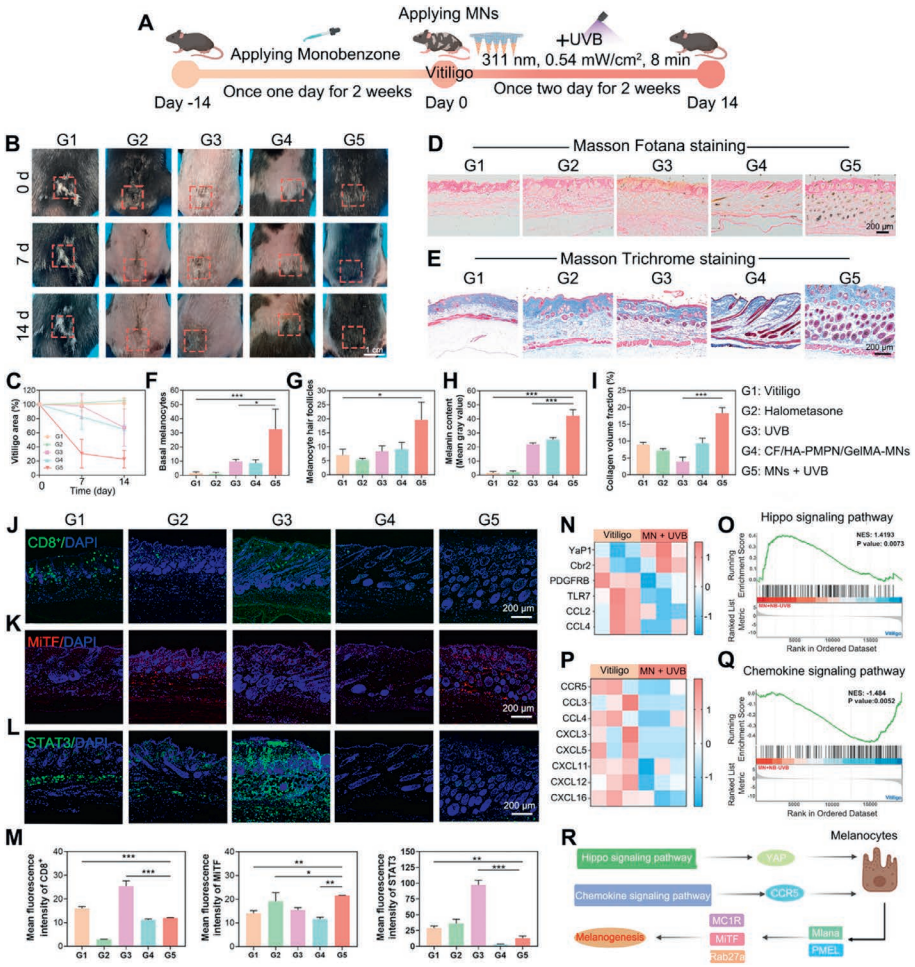


Fig. 3. Performance and biological mechanisms of CF/HA-PMPN/GelMA-MNs-enhanced NB-UVB therapy for the treatment of vitiligo *in vivo*. (A) Schematic illustration of CF/HA-PMPN/GelMA-MNs combined NB-UVB treatment against vitiligo and the time arrangement of the whole animal experiment. (B) Representative photographs of skin decolorization sites of vitiligo mice at different time points under different treatments. (C) Quantitative analysis of relative vitiligo area at different time points. (D) Masson-Fontana and (E) Masson Trichrome staining images of the skin after different treatments on day 14. Quantification of (F) melanin, (G) count of hair follicles per unit square centimeter area, (H) counts of melanocytes per unit square centimeter area of the basal lamina, and (I) CVF in different treatment groups. Immunofluorescence images of (J) $CD8^+$, (K) MiTF, and (L) STAT3 on mouse skin after the receipt of different treatments on day 14. (M) Semi-quantitative analysis of fluorescence intensity ($n = 3$). (N) DEGs involved in anti-inflammatory and antioxidant after NB-UVB and CF/HA-PMPN/GelMA-MNs treatment. (O) GSEA showed that the MN+UVB group of upregulated genomes was associated with resistance to oxidative stress. (P) DEGs involved in immunosuppression after NB-UVB and CF/HA-PMPN/GelMA-MNs treatment. (Q) GSEA showed that down-regulated genomes in the MN+UVB group were associated with immunosuppression. (R) Signaling pathway relationship diagram for NB-UVB and CF/HA-PMPN/GelMA-MNs treatment of vitiligo. Data are shown as mean ± SD ($n = 3$). $^*P < 0.05$, $^{**}P < 0.01$, $^{***}P < 0.001$.

an almost negligible presence of melanin in both the vitiligo and halometasone groups on day 14 (Fig. 3D). This observation may be attributed to the oxidative stress induced by monobenzone, which triggers a non-specific immune response, leading to the destruction of hair follicles and melanocytes [57]. Conversely, a modest increase in the quantity of black dots, indicative of melanin deposition, was noted in the UVB group, alongside a minor restoration of hair follicles and melanocytes in the MN group (Figs. 3F and G). Among the various treatment groups, the MN + UVB group demonstrated a significantly elevated number of melanocytes, an increased count of hair follicles, and a higher density of melanin deposition (Figs. 3F–H). These findings suggest that the synergistic application of NB-UVB light and the CF/HA-PMPN/GelMA-MNs yields the most pronounced effects on skin pigmentation in the mouse model of vitiligo. Moreover, Masson Trichrome staining indicated a significant reduction in the collagen volume fraction (CVF) within the UVB group compared to all other groups (Figs. 3E and I). This reduction suggests a decreased collagen content in the skin tissues of the mice, which might be due to the myriad cellular responses elicited by NB-UVB light, including oxidative stress, inflammation, and apoptosis. In contrast, the combined treatment of CF/HA-PMPN/GelMA-MNs with NB-UVB light resulted in a notable increase in both collagen content and the presence of mature hair follicles in the skin tissues of the treated mice due to the excellent antioxidant and anti-inflammatory ability of CF/HA-PMPN/GelMA-MNs. These findings underscore the beneficial effects of this combined therapeutic approach in promoting skin health and enhancing the structural integrity of the dermal matrix.

To further investigate the remodeling of the pathological microenvironment by the CF/HA-PMPN/GelMA-MNs, the antioxidant and anti-inflammatory mechanisms were evaluated by immunofluorescence staining for Nrf2 and TNF-α. As shown in Fig. S21 (Supporting information), the expression levels of Nrf2 were elevated in both MN group and MN+UVB group, suggesting activation of endogenous antioxidant defenses [58]. Meanwhile, the expression levels of TNF-α in the MN+UVB group were significantly lower than those observed in the other groups (Fig. S22 in Supporting information). Immunoregulatory capacity of CF/HA-PMPN/GelMA-MNs was further assessed through immunofluorescence staining of CD8. Given that the immune system is perturbed in vitiligo lesions, $CD8^+$ T cells become activated in a cytotoxic manner, leading to specific damage to melanocytes [59]. As shown in Fig. 3J, com-

pared with the vitiligo group, the $CD8^+$ expression was markedly elevated in the UVB group, which was because NB-UVB light irradiation may augment the activation and expression of cytotoxic proteins in $CD8^+$ T cells through mechanisms involving photooxidation [60]. MNs alone inhibited $CD8^+$ T cell infiltration to some extent, while the $CD8^+$ expression was significantly inhibited in the MN + UVB group, indicating that the NB-UVB irradiation could enhance the immune modulation of psoralen [33,36]. These findings indicate that the combined treatment of NB-UVB with CF/HA-PMPN/GelMA-MNs can effectively diminish the secretion of pro-inflammatory factors and $CD8^+$ T-cell infiltration, thereby aiding in the regulation of homeostasis within the microenvironment and promoting pigment deposition of vitiligo lesions.

The melanin synthesis in different treatment groups was evaluated by fluorescence staining of microphthalmia-associated transcription factor (MiTF). Compared with the vitiligo group, the expression of MiTF was notably elevated in all experimental groups, with the most pronounced expression observed in the MN + UVB group (Fig. 3K). This result indicates that the combination of NB-UVB light with CF/HA-PMPN/GelMA-MNs can enhance melanin deposition at the vitiligo lesion sites by modulating the expression of critical genes essential for the normal synthesis of melanin by melanocytes. This regulatory mechanism is believed to influence the processes of melanocyte differentiation, pigmentation, and proliferation, as highlighted in existing literature [16,61]. Furthermore, combination therapy substantially downregulated signal transducer and activator of transcription 3 (STAT3) expression without significantly affecting JAK2 levels (Fig. 3L and Fig. S23 in Supporting information), indicating selective inhibition of the STAT3 pathway as a key mechanism for breaking the inflammatory cascade in vitiligo pathogenesis. Quantitative analysis further revealed a similar trend with the fluorescence images (Fig. 3M). These findings collectively demonstrate the system's capacity to modulate multiple arms of vitiligo's pathological immune response while minimizing collateral immunomodulatory effects through pathway-selective intervention.

To gain further insight into the mechanisms by which CF/HA-PMPN/GelMA-MNs combined with NB-UVB facilitate skin repigmentation, transcriptome analyses were conducted. Comprehensive transcriptome analyses (principal component analysis, volcano plot, gene ontology/Kyoto encyclopedia of genes and genomes (GO/KEGG) enrichment) confirmed model reliability and highlighted pathways related to oxidative stress, immune regulation, and melanogenesis (Fig. S24 in Supporting information). In addition, hierarchical clustering analysis of differentially expressed genes (DEGs) showed significant upregulation of the antioxidant gene Yes-associated protein 1 (YAP1), a key Hippo-pathway effector mediating oxidative-stress responses [62,63], in the MN + UVB group (Fig. 3N). Meanwhile the MN + UVB group down-regulated oxidative stress-related genes, such as PDGFRB (phosphatidylinositol 3-kinase (PI3K)-Akt signaling pathway [64]) and Toll-like receptor 7 (TLR7, mitogen-activated protein kinase (MAPK) signaling pathway). Thus, it was shown that CF/HA-PMPN/GelMA-MNs and NB-UVB combination therapy protected melanocytes from monobenzone-induced oxidative stress damage mainly by modulating the Hippo-YAP pathway and regulating key genes in the PI3K-Akt signaling pathway and MAPK signaling pathway, thereby reducing oxidative stress products. Gene set enrichment analysis (GSEA) of these down- and up-regulated gene sets enriched in the MN + UVB group were involved in Hippo signaling pathway (Fig. 3O). Furthermore, the MN + UVB treatment group downregulated the expression of pro-inflammatory genes (CCL2 and CCL4) and upregulated the expression of the anti-inflammatory factor Cbr2 (Fig. 3N), suggesting that the combined treatment of CF/HA-PMPN/GelMA-MNs combined with UVB can exert a good anti-inflammatory effect and improve the inflammatory microenvironment of vitiligo lesions. In addition, the expression of genes related to immune overexpression (CCR5, CCL3, CCL4, CXCL3, CXCL5, CXCL11, CXCL12, and CXCL16) in the MN + UVB group was inhibited, with GSEA confirming downregulation of Chemokine signaling pathway (Figs. 3P and Q), suggesting that the combined treatment can regulate the vitiligo immune microenvironment and protect melanocytes from autoimmune damage by decreasing autoimmune-related correlates. Furthermore, the MN + UVB treatment upregulated the expression of genes related to melanogenesis that govern the melanocyte life cycle (SOX5, Mlana, PMEL, DCT, Wnt3a, POMC, KIT, MC1R, MiTF, TYRP1, TYR, and Rab27a) (Fig. S25 in Supporting information). Key regulators of melanocyte differentiation and melanogenesis, including SOX5, Mlana, PMEL, and DCT [65–68], were upregulated, and Wnt3a, which promotes both neural crest cell differentiation into melanocytes and MiTF upregulation in melanoblasts [65], was also upregulated. MiTF, a key transcription factor in melanogenesis, regulates genes including TYRP1. Upregulation of POMC further enhances MiTF expression, while receptors KIT and MC1R activate TYR, driving melanin synthesis. Together, TYR and TYRP1 catalyze tyrosine conversion into melanin within melanosomes, explaining how UVB phototherapy promotes melanogenesis [65–67]. The aforementioned results regarding the relevant genes underscore that the combination of UVB treatment and CF/HA-PMPN/GelMA-MNs is advantageous for promoting the regulation of the melanocyte life cycle and enhancing melanin synthesis in vitiligo-affected skin. Additionally, the utilization of the transporter protein Rab27a aids in the transport of melanosomes out of melanocytes, facilitating the re-pigmentation of vitiligo skin. According to the above results, it might be concluded that the combination of UVB and CF/HA-PMPN/GelMA-MNs contributes to a therapeutic effect in the treatment of vitiligo by mitigating oxidative stress, exerting immunomodulatory effect to inhibit autophagic damage to melanocytes, and promoting the secretion of melanin by melanocytes (Fig. 3R).

Current vitiligo treatments face significant limitations due to melanocyte dysfunction. While α-MSH therapy is constrained by its short half-life, enzymatic degradation, and need for frequent administration [69,70], it may also fail in cases of complete melanocyte loss (leucoderma), with efficacy further complicated by high interpatient variability. Therefore, it is necessitating optimized delivery systems to improve cost-effectiveness and long-term safety. Similarly, JAK inhibitors exhibit inconsistent responses, ranging from no repigmentation to partial effects, often followed by relapse upon discontinuation, alongside risks of immunosuppression-related infections and substantial financial burden due to lack of insurance coverage [71–73]. In contrast, the bilayer CF/HA-PMPN/GelMA-MNs patch combined the benefits of NB-UVB therapy while mitigating its phototoxicity through reduced ROS-mediated damage and enhanced collagen synthesis [74–77], simplifying post-treatment care to basic moisturization and sun protection for improved patient compliance. This innovative system enables differential dual release of Cur and psoralen, synergistically enhancing anti-inflammatory, antioxidant, immunemodulatory, and melanogenic effects beyond traditional therapies. The rapid repigmentation observed in monobenzone-induced vitiligo mice underscores its efficacy in restoring immune equilibrium and melanocyte function, presenting a clinically translatable solution that balances safety, convenience, and therapeutic impact for localized vitiligo and potential wider dermatological applications.

Declaration of competing interest

The authors declare that they have no known competing financial interests or personal relationships that could have appeared to influence the work reported in this paper.

CRediT authorship contribution statement

Wenxiu Hu: Writing – original draft, Validation, Methodology, Investigation, Formal analysis, Data curation, Conceptualization. **Di Liu:** Visualization, Investigation, Formal analysis, Conceptualization. **Jingxian Gao:** Visualization, Methodology, Formal analysis. **Xinyue Zhang:** Methodology, Formal analysis. **Qiqi Zhang:** Visualization, Investigation. **Lu Han:** Writing – review & editing, Supervision, Project administration, Methodology, Funding acquisition, Conceptualization.

Acknowledgments

This work was supported by Natural Science Fund for Excellent Young Scholars of Shandong Province (No. ZR2022YQ18), Fundamental Research Funds for Central-Universities (Nos. 202241010, 202212014), and Youth Innovation Team of Shandong Provincial Higher Education Institutions (No. 2022KJ048).

Supplementary materials

Supplementary material associated with this article can be found, in the online version, at doi:10.1016/j.cclet.2025.111877.

References

[1] M. Willemsen, N.F. Post, N.O.P. van Uden, et al., J. Invest. Dermatol. 142 (2022) 876–883 e3.
[2] M.L. Frisoli, K. Essien, J.E. Harris, Annu. Rev. Immunol. 38 (2020) 621–648.
[3] J. Chen, S. Li, C. Li, Med. Res. Rev. 41 (2021) 1138–1166.
[4] P. Kang, J. Chen, W. Zhang, et al., Cell Death. Discov. 8 (2022) 70.
[5] J.P. Strassner, J.E. Harris, Curr. Opin. Immunol. 43 (2016) 81–88.
[6] B.K. Khaitan, T. Sindhuja, Autoimmun. Rev. 21 (2022) 102932.
[7] S. Fatima, T. Abbas, M.A. Refat, et al., Int. J. Dermatol. 62 (2023) 279–289.
[8] X. Wu, Y. Yang, L. Xiang, C. Zhang, Pigm. Cell Melanoma Res. 34 (2021) 256–267.
[9] J. Tian, Y. Wang, M. Ding, et al., Oxid. Med. Cell Longev. 2021 (2021) 7617839.
[10] S. He, J. Xu, J. Wu, Oxid. Med. Cell Longev. 2022 (2022) 8796735.
[11] S. Maschalidi, F.E. Sepulveda, A. Garrigue, A. Fischer, G. de Saint Basile, Blood 128 (2016) 60–71.
[12] M. Rodrigues, K. Ezzedine, I. Hamzavi, et al., J. Am. Acad. Dermatol. 77 (2017) 1–13.
[13] J. Perez-Bootello, R. Cova-Martin, J. Naharro-Rodriguez, G. Segurado-Miravalles, Int. J. Mol. Sci. 24 (2023) 24.
[14] P.M. Moghadam, S.R. Rasouli, F. Gheybi, E. Karimi, S.Amir Hossein, Phytomedicine Plus 37666 (2023) 100437.
[15] B. Bellei, F. Papaccio, M. Picardo, Biomedicines 10 (2022) 2744.
[16] S. Chong, C. Wei, L. Feng, R. Guo, ACS Biomater. Sci. Eng. 9 (2023) 3368–3378.
[17] W. Choi, Y. Miyamura, R. Wolber, et al., J. Invest. Dermatol. 130 (2010) 1685–1696.
[18] S.A.M. Salem, N.S. Ahmed, M.Y. Ahmed, W.M. Seoudy, O.M.A. Ahmed, QJM: Int. J. Med. 114 (2022) hcab093-039.
[19] R. Speeckaert, E.V. Caelenberg, A. Belpaire, M.M. Speeckaert, N.V. Geel, J. Clin. Med. 13 (2024) 5225.
[20] F. Touma, M. Lambert, A. Martinez Villarreal, et al., Biomedicines 11 (2023) 3017.
[21] L.L. Li, C.L. Guo, Y.L. Fang, et al., Chin. Chem. Lett. 36 (2025) 110839.
[22] Q.X. Tan, E. Pang, Q. Wang, et al., Chin. Chem. Lett. 36 (2025) 110770.
[23] J. Yang, B. Yang, J. Shi, Angew. Chem. Int. Ed. 62 (2023) e202310061.
[24] I.H. Ibeogu, H.K. Bako, M.S. Yar, et al., Food Hydrocoll. 149 (2024) 109617.
[25] S. Almatroodi, A. Rahmani, J. Thorac. Oncol. 15 (2020) S26.
[26] Y.C. Liu, Y.K. Lin, Y.T. Lin, et al., Adv. Sci. 11 (2024) e2308635.
[27] L. Qi, J. Jiang, J. Zhang, L. Zhang, T. Wang, Antioxidants 9 (2020) 121.
[28] S. Gao, X. Duan, X. Wang, et al., Food Chem. Toxicol. 59 (2013) 739–747.
[29] X. Yang, H. Jiang, Y. Shi, Cell Biosci. 7 (2017) 20.
[30] H. Ruan, Q. Huang, B. Wan, M. Yang, Inflammopharmacology 30 (2022) 517–525.
[31] W. Luo, L. Bai, J. Zhang, et al., Carbohydr. Polym. 311 (2023) 120718.
[32] H. Liang, X. Sun, J. Gao, B. Zhou, Int. J. Biol. Macromol. 165 (2020) 2267–2274.
[33] P. Galiatsatos, D.D. Maydan, E. Macalpine, et al., J. Cancer Res. Clin. Oncol. 150 (2024) 130.
[34] L. Yin, G. Pang, C. Niu, et al., Int. J. Mol. Med. 41 (2018) 3727–3735.
[35] S. Doppalapudi, S. Mahira, W. Khan, J. Photochem. Photobiol. B 174 (2017) 44–57.
[36] J. Diekmann, I. Theves, K.A. Thom, P. Gilch, Molecules 25 (2020) 5242.
[37] S.A. Birlea, G.E. Costin, D.R. Roop, D.A. Norris, Med. Res. Rev. 37 (2017) 907–935.
[38] Y. Sun, M.L. Chen, Y. Chen, et al., Chin. Chem. Lett. 36 (2025) 110908.
[39] Z. Li, P. Zhao, Z. Ling, et al., Adv. Healthc. Mater. 13 (2024) e2302406.
[40] C. Caudill, J.L. Perry, K. Iliadis, et al., Proc. Natl. Acad. Sci. U. S. A. 118 (2021) e2102595118.
[41] Z. Zhao, A. Ukidve, A. Dasgupta, S. Mitragotri, Adv. Drug Deliv. Rev. 127 (2018) 3–19.
[42] Q. Bian, Y.H. Xu, X.L. Ma, et al., Adv. Funct. Mater. 32 (2022) 32.
[43] B. Mbituyimana, M. Adhikari, F. Qi, et al., J. Control. Release 362 (2023) 692–714.
[44] X.C. Li, L. Guan, X.L. Li, et al., Chin. Chem. Lett. 36 (2024) 110661.
[45] J. Liu, H. Liu, S. Huang, et al., Small 20 (2024) e2309583.
[46] L.P. Yuan, M. Pan, H.Z. Deng, et al., Chin. Chem. Lett. 36 (2024) 110723.
[47] X.R. Xi, X.Y. Wang, Z.Y. Xi, et al., Chin. Chem. Lett. 36 (2024) 110773.
[48] S. Wong, J. Zhao, C. Cao, et al., Nat. Commun. 10 (2019) 582.
[49] J. Wan, F. Lin, W. Zhang, et al., Int. J. Biol. Sci. 13 (2017) 391–400.
[50] W. Lu, C. Kong, S. Cheng, X. Xu, J. Zhang, Int. J. Biol. Macromol. 235 (2023) 123717.
[51] M.C. Sun, X.L. Xu, Y. Du, et al., ACS Nano 15 (2021) 17361–17374.
[52] W. Yang, W. Zhong, S. Yan, et al., Adv. Mater. 36 (2024) e2312740.
[53] Y.Q. Liang, S.L. Li, Y.X. Pan, et al., Chin. Chem. Lett. 36 (2025) 110841.
[54] X.C. Li, D. Mo, S.X. Hu, et al., Chin. Chem. Lett. 36 (2024) 110674.
[55] L. An, D. Kim, L.R. Donahue, et al., Nat. Commun. 15 (2024) 796.
[56] Y. Ahn, J. Seo, E.J. Lee, et al., J. Invest. Dermatol. 140 (2020) 1794–1804.e4.
[57] S. Luo, X. Meng, J. Ai, et al., Int. J. Mol. Sci. 25 (2024) 3411.
[58] Y. Lin, Y. Ding, Y. Wu, et al., Exp. Dermatol. 33 (2024) e14856.
[59] S. Li, G. Zhu, Y. Yang, et al., J. Allergy Clin. Immunol. 140 (2017) 177–189 e9.
[60] X. Chen, W. Guo, Y. Chang, et al., Free Radic. Biol. Med. 139 (2019) 80–91.
[61] H.M. Wang, L.Q. Qu, J.P.L. Ng, et al., Phytomedicine 98 (2022) 153941.
[62] D. Shao, P. Zhai, D.P. Del Re, et al., Nat. Commun. 5 (2014) 3315.
[63] Q. Liu, S. Pan, P. Li, R.A.F. Dixon, Sci. Rep. 13 (2023) 2232.
[64] W.S. Peng, M. Gao, X.F. Yao, et al., Anim. Sci. J. 94 (2023) e13891.
[65] S.A. D'Mello, G.J. Finlay, B.C. Baguley, M.E. Askarian-Amiri, Int. J. Mol. Sci. 17 (2016) 17.
[66] C. Regazzetti, F. Joly, C. Marty, et al., J. Invest. Dermatol. 135 (2015) 3105–3114.
[67] S. Zhou, H. Zeng, J. Huang, et al., Ageing Res. Rev. 69 (2021) 101349.
[68] X. Yuan, D. Meng, P. Cao, et al., Dermatol. Ther. 32 (2019) e13025.
[69] C.L. Chang, Z.Q. Cai, S.Y.T. Hsu, Eur. J. Pharmacol. 958 (2023) 176008.
[70] J.Y. Liang, Y.H. Yu, C.X. Li, et al., Carbohydr. Polym. 305 (2023) 120549.
[71] The Lancet Rheumatology, Lancet Rheumatol. 6 (2024) e129.
[72] S. Inoue, T. Suzuki, S. Sano, I. Katayama, J. Dermatol. Sci. 113 (2024) 86–92.
[73] D.P. McLornan, J.E. Pope, J. Gotlib, C.N. Harrison, Lancet 398 (2021) 803–816.
[74] K. Zhang, G. Anumanthan, S. Scheaffer, L.A. Cornelius, J. Invest. Dermatol. 139 (2019) 202–212.
[75] D. Hao, X. Wen, L. Liu, et al., Cell Death. Dis. 10 (2019) 19.
[76] Y.J. Chen, N. Lian, S.H. Chen, et al., Cell Death. Dis. 13 (2022) 841.
[77] K.F. Akhter, M.A. Mumin, E.M.K. Lui, P.A. Charpentier, Int. J. Biol. Macromol. 181 (2021) 221–231.